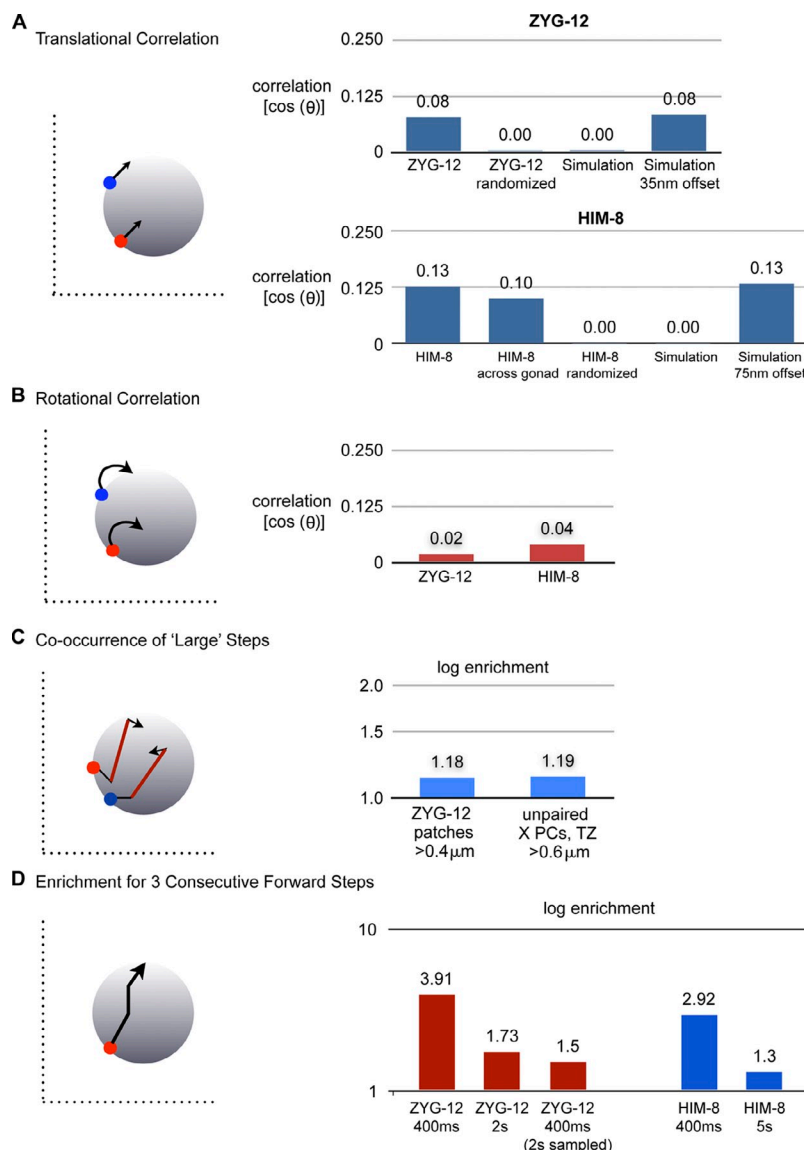Figure S1. **Assessment of correlations in motion data.** We analyzed our data to assess whether our imaging conditions or image alignment approach might have introduced artifacts that would impact our ability to measure or interpret the motion of fluorescent foci. For example, upward curvature in the MSD plot of patches could potentially be an artifact of physical drift of the sample that was not corrected by computational alignment. (A and B) First, to determine whether the observed motion of different foci showed any systematic correlations caused by image shifts or nuclear rotations, we measured the translational and rotational correlation of foci within individual nuclei and also among all foci within each dataset. These analyses were performed by analyzing sets of vectors describing all motions that occurred simultaneously. (A) Translational correlation was measured among concurrent steps of all ZYG-12::GFP foci (top) or between unpaired GFP::HIM-8 foci (bottom) within individual nuclei. Correlation is expressed as the mean of the cosines of all angles between concurrent steps in each nucleus. No correlation would yield a value of 0, whereas perfect correlation would result in value of 1. As expected, correlation within randomized datasets (vectors from randomized time intervals) showed no correlation. Because alignment for GFP::HIM-8 data was performed on whole fields of nuclei (see Materials and methods), we could also measure correlation among all X PCs in each dataset. The correlation of motion of all HIM-8 foci in each field was similar to the correlation within each nucleus, suggesting that the apparent correlation resulted from imperfect spatial alignment between adjacent time points. To estimate the magnitude of apparent displacement introduced by misalignment, we artificially introduced xyz offsets into the randomized datasets. We found that the degree of correlation we measured could be recapitulated by introducing translations of 35 and 75 nm in each dimension for each ZYG-12::GFP or GFP::HIM-8 step, respectively. Compared with a voxel size of 132 × 132 × 250 nm for ZYG-12::GFP (collected on the OMX system) or 114 × 114 × 500 nm for GFP::HIM-8 (on the spinning-disk confocal), these are nominal errors in registration that do not impact the conclusions of this work. (B) Rotational correlation was calculated using an approach similar to that described for translational correlation but was preceded by rotating tracks along a 3.5-µm-diameter sphere to confer maximal overlap of the preceding step. The minute correlations observed for both ZYG-12::GFP and GFP::HIM-8 indicate that nuclear rotation makes a negligible contribution to the observed displacements of PCs.

A Translational Correlation

ZYG-12

correlation [cos (θ)]

0.08 0.00 0.00 0.08

ZYG-12 | ZYG-12 randomized | Simulation | Simulation 35nm offset

HIM-8

correlation [cos (θ)]

0.13 0.10 0.00 0.00 0.13

HIM-8 | HIM-8 across gonad | HIM-8 randomized | Simulation | Simulation 75nm offset

B Rotational Correlation

correlation [cos (θ)]

0.02 0.04

ZYG-12 | HIM-8

C Co-occurrence of 'Large' Steps

log enrichment

1.18 1.19

ZYG-12 patches >0.4µm | unpaired X PCs, TZ >0.6µm

D Enrichment for 3 Consecutive Forward Steps

log enrichment

3.91 1.73 1.5 2.92 1.3

ZYG-12 400ms | ZYG-12 2s | ZYG-12 400ms (2s sampled) | HIM-8 400ms | HIM-8 5s

(C) We tested whether PCMs tend to occur independently by measuring the frequency of simultaneous large steps in the same nucleus (>0.4 µm for ZYG-12::GFP and >0.6 µm for unpaired TZ GFP::HIM-8 signals) and comparing this value to the expected number of co-occurrences, which was calculated by temporally randomizing the steps. The values close to 1 are consistent with independent movement of patches or X PCs in the same nucleus. (D) We assessed how frequently we captured multiple steps in the same direction as a function of the image acquisition interval. This is expressed as a ratio of the number of occurrences of three consecutive forward steps for each patch (turns <30° between each segment) over the number expected, based on temporally randomized data. The larger frequency of consecutive steps in the same direction in the ZYG-12::GFP data collected at 400-ms intervals versus 2 s indicates that such motions frequently lasted <6 s or three of the longer intervals. As expected, this enrichment is absent from the 400-ms dataset when undersampled to mimic the 2-s dataset (every fifth data point). Finally, similar levels of enrichment are observed for the GFP::HIM-8 in TZ nuclei when comparing 400-ms and 5-s data.
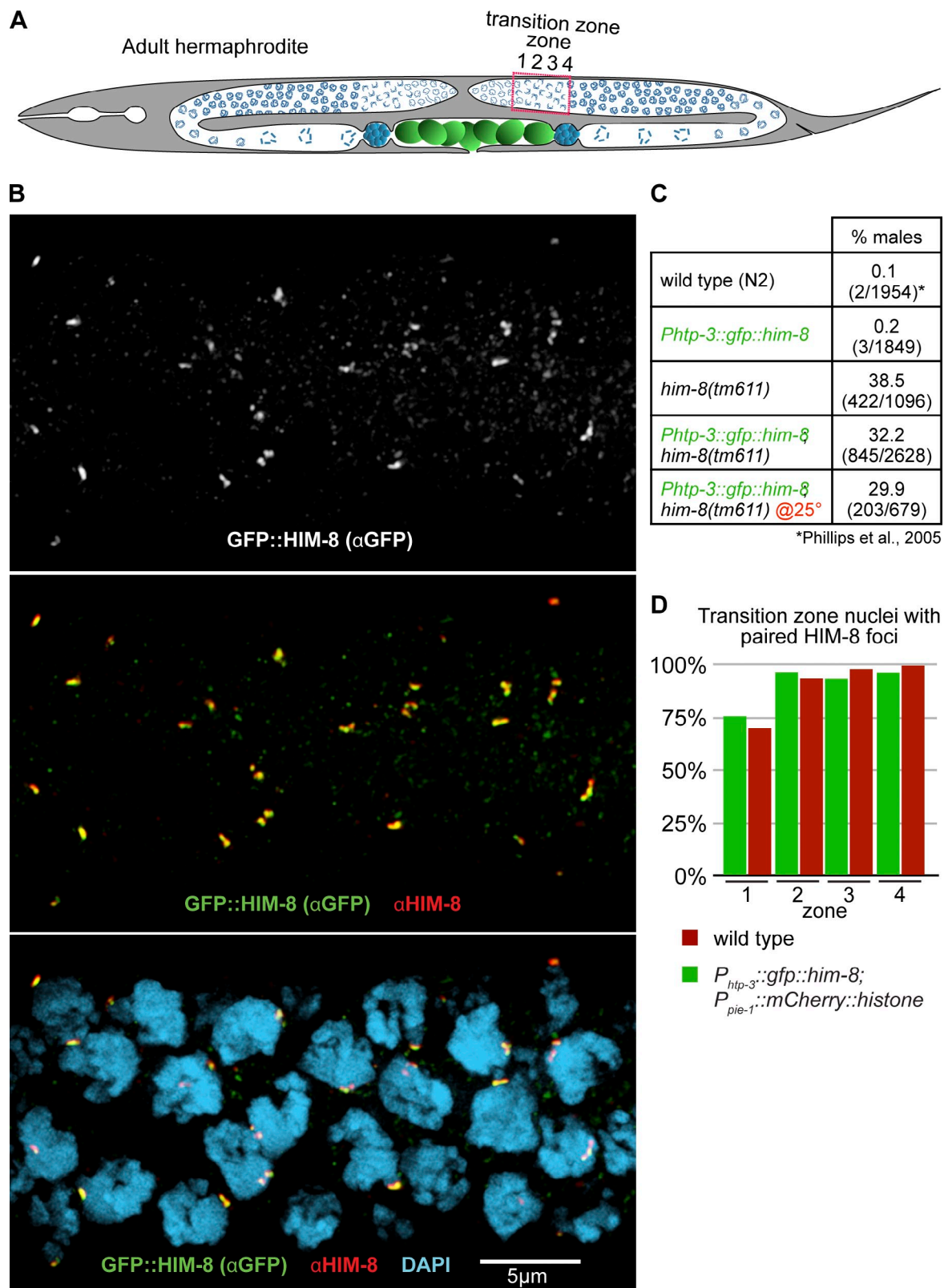
A

Adult hermaphrodite

transition zone
zone
1 2 3 4

B

GFP::HIM-8 (αGFP)

GFP::HIM-8 (αGFP)   αHIM-8

GFP::HIM-8 (αGFP)   αHIM-8   DAPI   5μm

C

	% males
wild type (N2)	0.1 (2/1954)*
Phtp-3::gfp::him-8	0.2 (3/1849)
him-8(tm611)	38.5 (422/1096)
Phtp-3::gfp::him-8 *him-8(tm611)*	32.2 (845/2628)
Phtp-3::gfp::him-8 *him-8(tm611)* @25°	29.9 (203/679)

*Phillips et al., 2005

D

Transition zone nuclei with paired HIM-8 foci

zone 1 2 3 4

◼ wild type

◼ P_{htp-3}::gfp::him-8; P_{pie-1}::mCherry::histone

Figure S2.   **GFP::HIM-8 localizes to the X PC and does not interfere with X chromosome pairing or segregation.** (A) Diagram of an adult *C. elegans* hermaphrodite indicating the temporospatial organization of germline nuclei. The rectangle indicates the TZ region imaged in B and the zones in which pairing was quantified in D. (B) Fixed TZ nuclei stained with antibodies against GFP and HIM-8 and counterstained with DAPI. Bar, 5 µm. (C) Frequency of male self-progeny, as a measure of X chromosome nondisjunction, from hermaphrodites expressing GFP::HIM-8 (P_{htp-3}::gfp::him-8). (D) Quantification of X PC pairing in animals expressing GFP::HIM-8 and mCherry::histone. The TZ regions of three gonads were divided into four sections of equal length, and pairing was quantified as described in the Materials and methods section (*n* = 3 gonads quantified for each genotype).
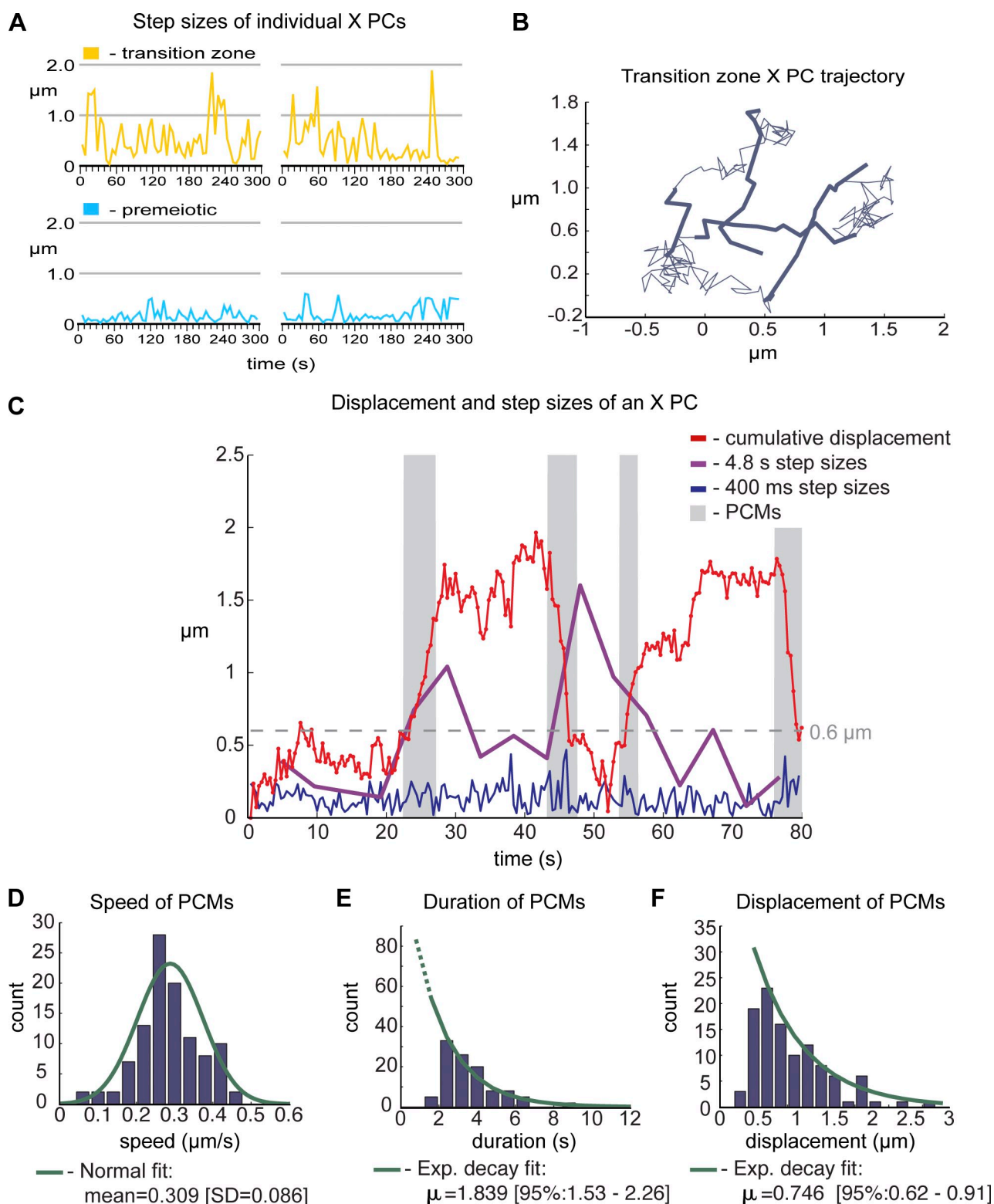
Figure S3. **Large X PC steps reflect PCMs.** (A) Colored tracks show step sizes of X PCs over the 5-min data collection in two representative TZ and premeiotic zone nuclei. (B) Trajectory of a single, representative X PC followed at 400-ms intervals (bold segments denote PCMs). (C) Cumulative displacement plot for the single trajectory shown in B. (D) Speed distribution of X PC PCMs. Mann–Whitney *U* test compared with the ZYG-12::GFP distribution, P = 2 × 10^{-18}. *n* = 131 PCMs. (E) Duration distribution of X PC PCMs. Fitted exponential (Exp.) decay is shown; dotted line shows extrapolation. Mann–Whitney *U* test compared with the ZYG-12::GFP distribution, P = 0.93. (F) Total displacement distribution of X PC PCMs. Mann–Whitney *U* test compared with the ZYG-12::GFP distribution, P = 4 × 10^{-9}.
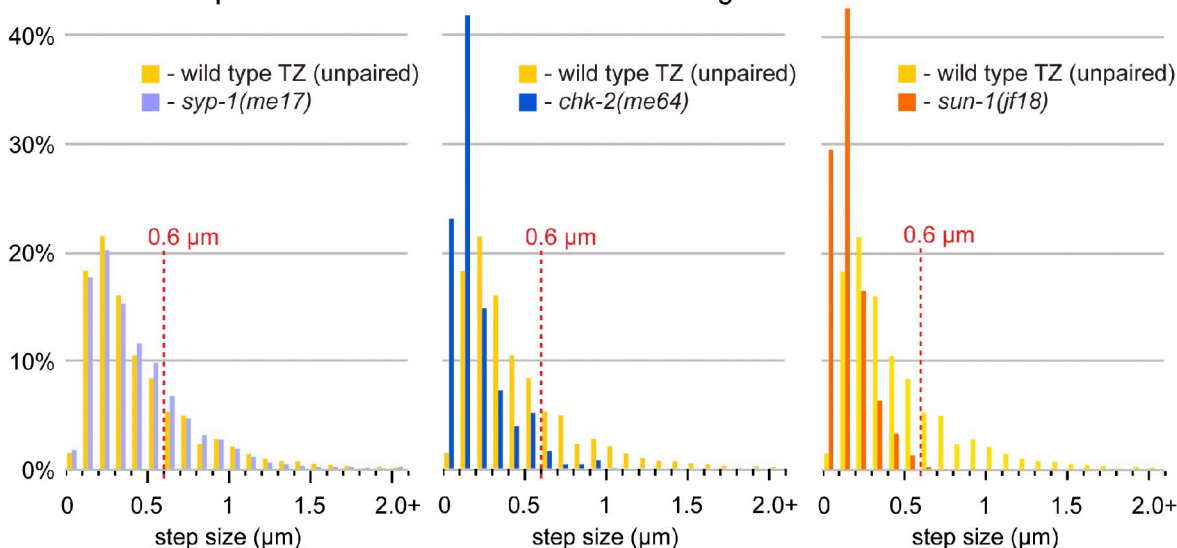
A Normalized step size distribution for HIM-8 vs. resampled ZYG-12 data
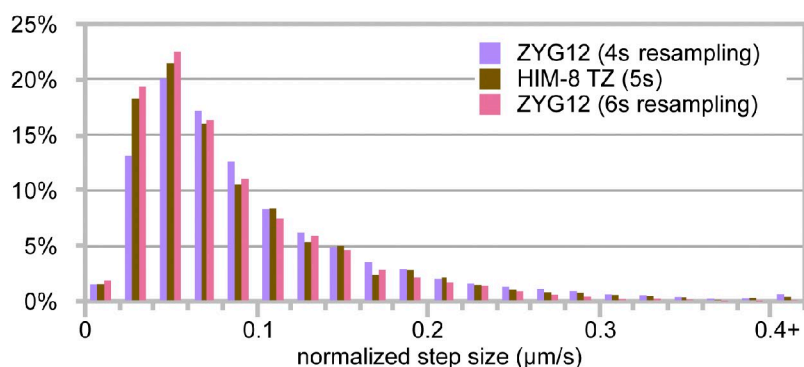
B Distributions of step sizes for wild type pachytene nuclei shown in Fig. 4 D and E
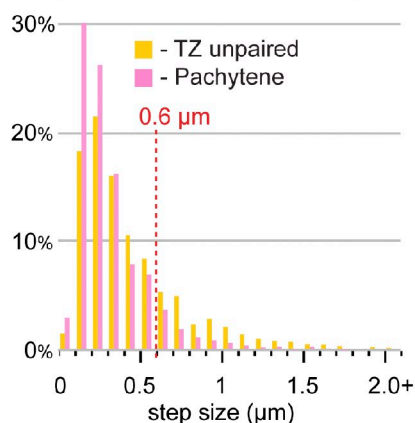
C Distributions of step sizes for mutant conditions shown in Fig. 4 D and E
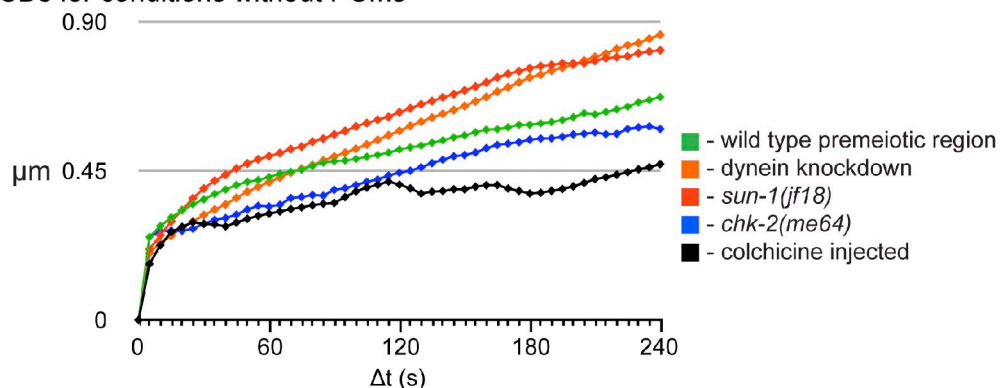
D Comparison of RMSDs for conditions without PCMs

Figure S4. **Additional comparisons of step-size distributions and RMSD plots.** (A) Histograms of normalized step sizes from HIM-8 trajectories ($n = 1,443$ steps) and from ZYG-12 trajectories imaged at 2-s intervals ($n = 7,663$ steps) but resampled at 4 and 6 s. Note that the HIM-8 step-size distribution lies between the 4- and 6-s ZYG-12 distributions, as expected based on the 5-s image intervals used for HIM-8 recordings. (B) Distributions of step sizes for X PCs in WT TZ nuclei compared with pachytene nuclei (Mann–Whitney U test, $P = 2 \times 10^{-62}$). (C) Distributions of step sizes for X PCs in WT TZ nuclei compared with TZ nuclei in syp-1(me17) animals (Mann–Whitney U test, $P = 0.5$), chk-2(me64) animals (Mann–Whitney U test, $P = 7 \times 10^{-86}$), and sun-1(jf18) animals (Mann–Whitney U test, $P = 9 \times 10^{-303}$). (D) Comparison of RMSD plots of X PC trajectories for WT premeiotic zone, chk-2(me64) mutant animals (Fig. 4), sun-1(j18) mutant animals (Fig. 4), colchicine-injected animals (Fig. 5), and dynein knockdown animals (dlc-1 RNAi in dhc-1(or195ts); Fig. 6).
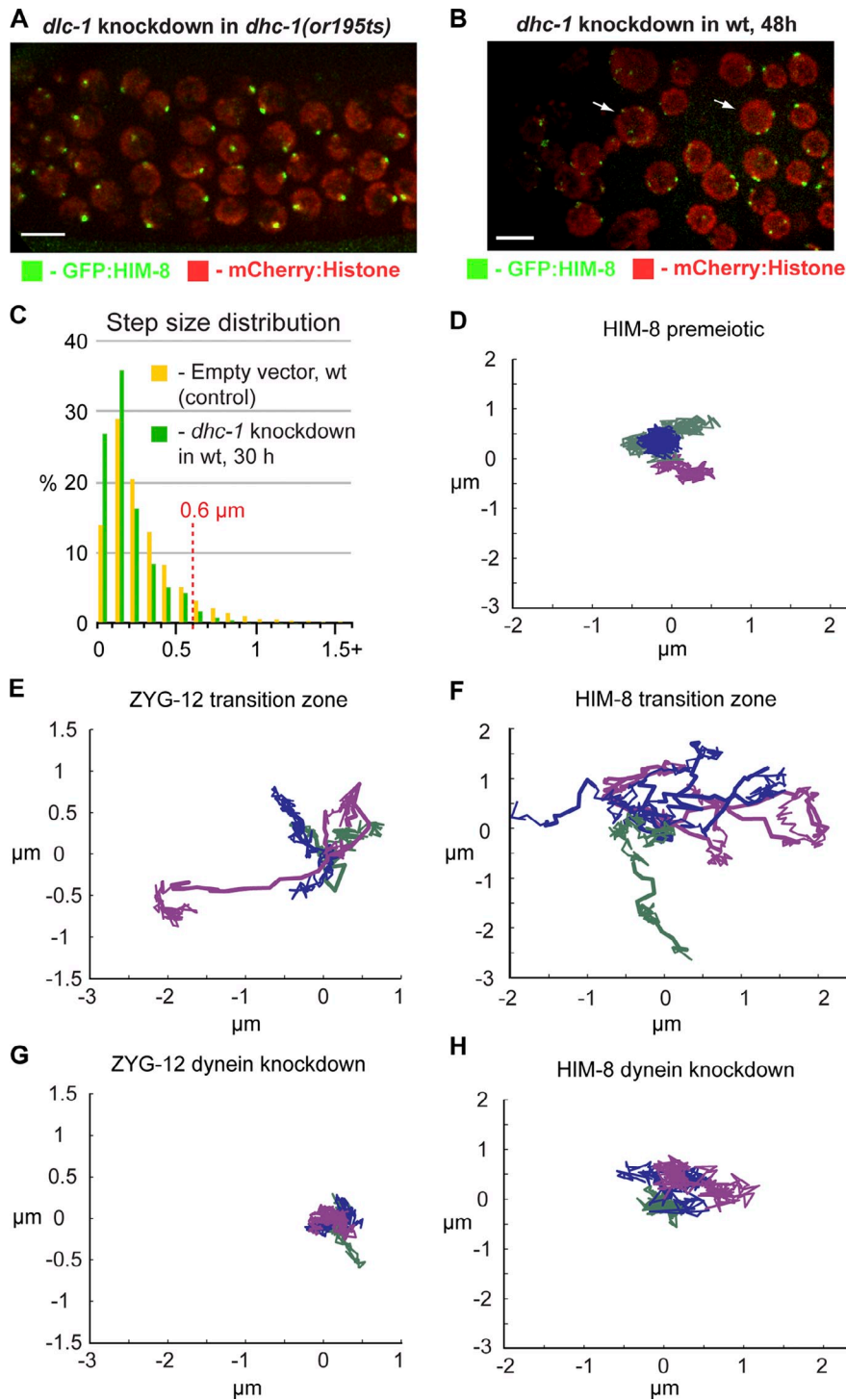
A *dlc-1* knockdown in *dhc-1(or195ts)*

■ - GFP:HIM-8   ■ - mCherry:Histone

B *dhc-1* knockdown in wt, 48h

■ - GFP:HIM-8   ■ - mCherry:Histone

C

Step size distribution

■ - Empty vector, wt (control)

■ - *dhc-1* knockdown in wt, 30 h

0.6 µm

D HIM-8 premeiotic

E ZYG-12 transition zone

F HIM-8 transition zone

G ZYG-12 dynein knockdown

H HIM-8 dynein knockdown

Figure S5. **PCMs are eliminated by dynein knockdown using different experimental approaches.** (A and B) Projection images showing GFP::HIM-8 and mCherry::histone in TZ nuclei from animals in which dynein function was reduced either by RNAi of dynein light chain (*dlc-1*) in dynein heavy chain (*dhc-1(or195ts)*) mutant animals at the restrictive temp for 24 h (A) or RNAi of dynein heavy chain (*dhc-1*) for 48 h in WT animals (B). Note that after 48 h of *dhc-1* knockdown, there are significant morphological defects (e.g., large polyploid nuclei with more than two GFP::HIM-8 foci [white arrows] and disorganized nuclear positioning) caused by mitotic defects in the premeiotic region of the gonad. Meiotic progression is from left to right. Bars, 5 µm. A disadvantage of this protocol is that animals must be kept at a restrictive temperature and subjected to RNAi for an extended period as adults, resulting in aging by a full day at 25°C relative to the animals imaged in our other experiments. As seen in the controls in Fig. 6, the aging and/or elevated temperature resulted in somewhat lower levels of PCMs than in younger animals (compare with Figs. 4 and 5). However, we found that RNAi-mediated knockdown of *dhc-1* alone, which did not require elevated temperatures or extended time as adults, also resulted in loss of PCMs. However, this approach causes more severe defects in germline mitosis than the double knockdown, resulting in polyploid meiotic nuclei with multiple GFP::HIM-8 foci (not depicted). (C) Distributions of step sizes in the TZ of dynein knockdown animals using RNAi of *dhc-1* in WT animals for 30 h compared with TZ step sizes in RNAi control animals (*dlc-1* RNAi in *dhc-1(or195ts)*: 2,599 steps, 45 trajectories, and 3 datasets; control RNAi: 2,588 steps, 45 trajectories, and 3 datasets). Bins = 0.1 µm. (D–H) Trajectories of three ZYG-12 patches (E and G) or HIM-8 foci (D, F, and H) followed at 400-ms intervals from premeiotic nuclei in WT animals (D), TZ nuclei in WT animals (E and F), and dynein knockdown (*dlc-1* RNAi in *dhc-1(or195ts)*) animals (G and H). Each color represents an individual trajectory, and bold segments denote PCMs.
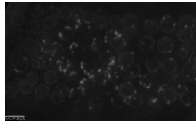
Video 1. **3D time-lapse imaging reveals ZYG-12::GFP patch motions along the NE.** The first sequence (2–4 s) shows 3D time-lapse imaging of a hermaphrodite worm expressing ZYG-12::GFP. The field of view spans the entire TZ region of the gonad shown in Fig. 1 C, with premeiotic nuclei shown on the left and some nuclei that have progressed into pachytene shown on the right. Projections of stacks of optical sections acquired every 2 s on the OMX imaging system are played back at 25 fps (50× real time). Bar, 5 μm. The second sequence (from 6 s to the end) shows a rotating animation of the same dataset to highlight the 3D image reconstruction. Large tick marks indicate 5 μm. Time is given in minutes and seconds.
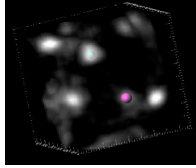

Video 2. **ZYG-12::GFP patches exhibit heterogeneous, independent trajectories.** The first two sequences (2–6 and 8–13 s) show a single TZ nucleus (corresponding to Fig. 1, D and E) in which merging and splitting of ZYG-12::GFP patches over time is apparent. The third and fourth sequences (15–20 and 22 s to the end) show a single TZ nucleus (corresponding to Fig. 1, F and G) in which six ZYG-12::GFP foci exhibit independent motions. Both pairs of sequences show nuclei with and without spheres (0.4-μm diameter) that indicate the automatically tracked positions. For all, projections of stacks of optical sections acquired every 2 s using the OMX imaging system are played at 12.5 fps (25× real time). Large tick marks indicate 1 μm.
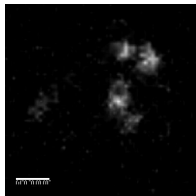

Video 3. **PC motion at higher temporal resolution using ZYG-12::GFP.** Related to Fig. 2. A TZ nucleus expressing ZYG-12::GFP from a 2D dataset acquired using a spinning-disk confocal microscope. A single confocal image plane near the apical surface of the nucleus was imaged every 400 ms using a spinning-disk confocal microscope and played back at a frame rate of 62.5 fps (25× real time). Bar, 1 μm. Time is given in minutes and seconds.
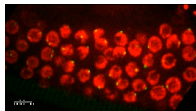

Video 4. **Imaging of GFP::HIM-8 reveals rapid motion of the X PCs.** 3D time-lapse imaging of a hermaphrodite expressing GFP::HIM-8 (green) and mCherry::histone (red) and corresponding to Fig. 3 A. The field of view shows the entire TZ region, with premeiotic nuclei shown on the left and some nuclei that have progressed into pachytene shown toward the right. Projections of stacks of confocal sections acquired every 5 s using a spinning-disk confocal microscope are played at 10 fps (50× real time). Bar, 5 μm. Time is given in minutes and seconds.
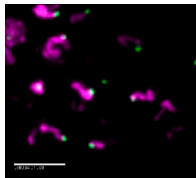

Video 5. **GFP::HIM-8 and X chromosome labeling reveal that chromosome motion is mediated by the PC.** Related to Fig. 3. GFP::HIM-8 (green) and Cy5 (purple; enriched on the X chromosomes) in the TZ region of the gonad. In the first sequence (2–8 s) the field of view shows a portion of the TZ region. In the second sequence (10 s to the end), the field of view shows a single nucleus in which dramatic, end-driven chromosome motion is apparent. Projections of stacks of confocal sections acquired every 5 s using a spinning-disk confocal microscope are played at 10 fps (50× real time). Bar, 5 μm. Time is given in minutes and seconds.
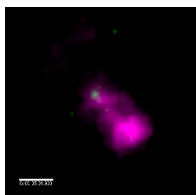

Video 6. **Chromosome elasticity is revealed by imaging of GFP::HIM-8, and X chromosome labeling shows chromosome elasticity.** GFP::HIM-8 (green) and Cy5 (purple; labeling the X chromosome) shown in a field of view that highlights a single nucleus in the TZ (corresponding to Fig. 3 C) in which the GFP::HIM-8 focus moves far away from the remainder of the X chromosome. Projections of stacks of confocal sections acquired every 5 s using a spinning-disk confocal microscope are played at 10 fps (50× real time). Bar, 1 μm. Time is given in minutes and seconds.
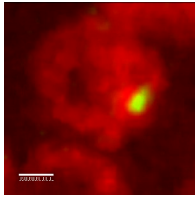
Video 7.   **During rapid motions, PCs undergo extensive stretching.** GFP::HIM-8 (green) and mCherry::histone (red) shown in a field of view that highlights a single nucleus in the TZ (corresponding to Fig. 3 D) in which the GFP::HIM-8 focus displays transient stretching. Projections of stacks of confocal sections acquired every 5 s using a spinning-disk confocal microscope are played at 10 fps (50× real time). Bar, 1 µm. Time is given in minutes and seconds.
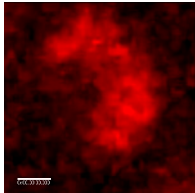
Video 8.   **Paired X PCs can separate for up to several seconds before reassociating.** GFP::HIM-8 (green) and mCherry::histone (red) shown in a field of view that highlights a single nucleus in the TZ (corresponding to Fig. 3 E) in which the GFP::HIM-8 foci become unpaired after colocalizing. Projections of stacks of confocal sections acquired every 5 s using a spinning-disk confocal microscope are played at 10 fps (50× real time). Bar, 1 µm. Time is given in minutes and seconds.
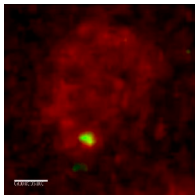
Video 9.   **X PC motion in representative nuclei from the TZ or premeiotic regions.** GFP::HIM-8 (green) and mCherry::histone (red) shown in a field of view that highlights a single nucleus in the TZ in which X PCs are unpaired (first sequence, 2–8 s; corresponding to Fig. 4 A, top) or a single nucleus in the premeiotic region (second sequence, 10 s to the end; corresponding to Fig. 4 A, bottom). Projections of stacks of confocal sections acquired every 5 s using a spinning-disk confocal microscope are played at 10 fps (50× real time). Bar, 1 µm. Time is given in minutes and seconds.
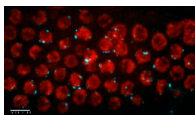
Video 10.   **The motion of dynein at NE patches using GFP::DHC-1 and the reduction in X PC motion after inhibition of dynein by RNAi.** First sequence (2–8 s): DHC-1::GFP (cyan) and mCherry::histone (red) in the TZ region of the gonad (corresponding to Fig. 6 A). Second sequence (10 s to the end): GFP::HIM-8 (green) and mCherry::histone (red) in the TZ region of an animal with compromised dynein function (*dhc-1(or195)*; *dlc-1(RNAi)*). Fields of view show the entire TZ region with nuclei that have progressed further in meiosis on the right. Projections of stacks of confocal sections acquired every 5 s using a spinning-disk confocal microscope are played at 10 fps (50× real time). KD, knockdown. Bar, 5 µm. Time is given in minutes and seconds.

Reference

Phillips, C.M., C. Wong, N. Bhalla, P.M. Carlton, P. Weiser, P.M. Meneely, and A.F. Dernburg. 2005. HIM-8 binds to the X chromosome pairing center and mediates chromosome-specific meiotic synapsis. *Cell*. 123:1051–1063. http://dx.doi.org/10.1016/j.cell.2005.09.035